GSA Data Repository 2018002

Chen et al., 2018, Dehydration of phengite inferred by electrical conductivity measurements: Implication for the high conductivity anomalies relevant to the subduction zones: Geology, https://doi.org/10.1130/G39716.1

APPENDIX. SUPPLEMENTARY FIGURES AND TABLE

This appendix file includes:

(1) Figure DR1. Schematic cross-section of the cell assembly for electrical conductivity measurements;

(2) Figure DR2. Representative electron backscattered images of the recovered samples prior to and following phengite dehydration;

(3) Figure DR3. Impedance spectrum of phengite prior to and during its dehydration;

(4) Figure DR4. Comparison between electrical conductivity of phengite and other minerals;

(5) Figure DR5. Comparison between the conductivity values recorded by MT surveys and experimental result following phengite breakdown;

(6) Table DR1. Chemical compositions of the starting material and the run products;

(7) References.

20

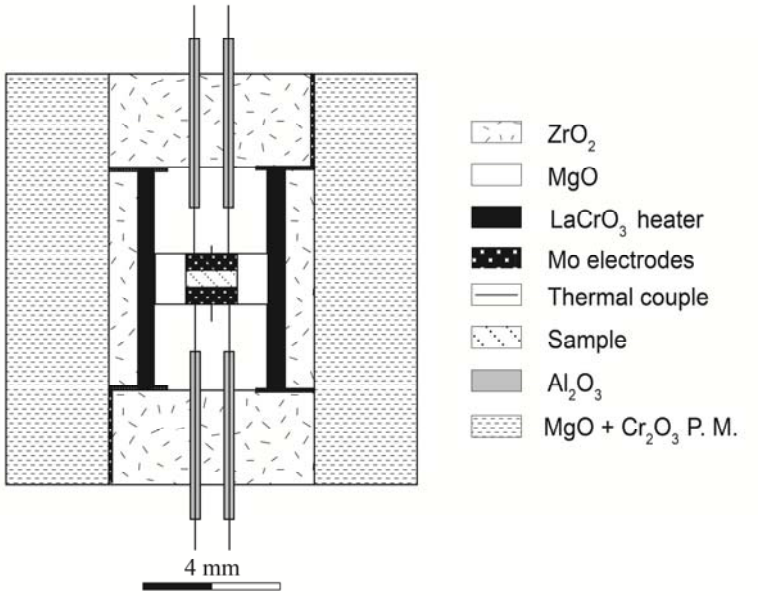

21

22 Figure DR1. Schematic cross-section of the cell assembly for electrical conductivity

23 measurements.

24

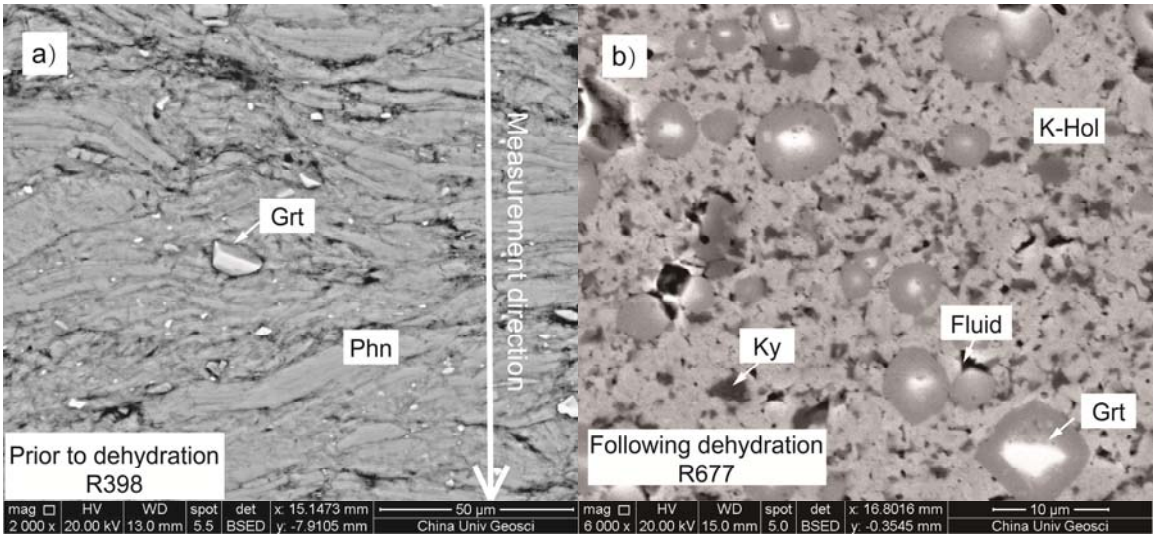

Figure DR2. Representative electron backscattered images of the recovered samples prior to and following phengite dehydration. (a) The recovered sample prior to its dehydration (run R398). Phengite (Phn) and garnet (Grt) are shown in the figure. (b) The recovered sample following its dehydration (run R677). The pores (dark regions) should be filled by fluids released from phengite breakdown. K-hollandite (K-Hol) and kyanite (Ky) are shown by light-grey and dark-grey, respectively. Composition zoning occurred during 1 h annealing at temperatures between 950 and 1200 K.

35

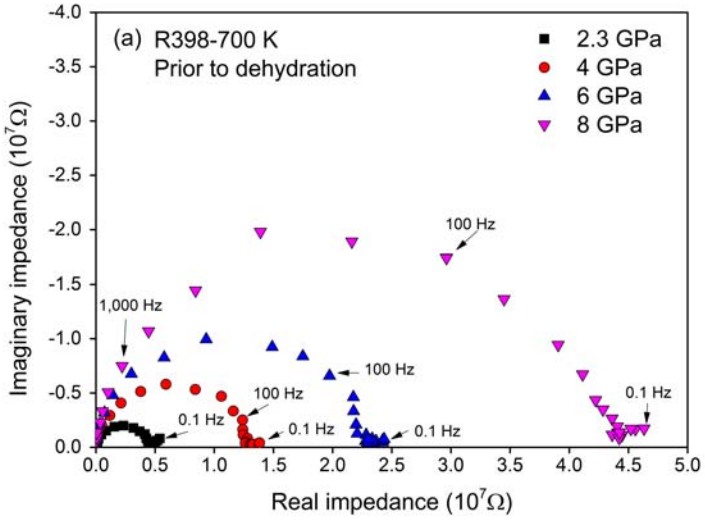

36

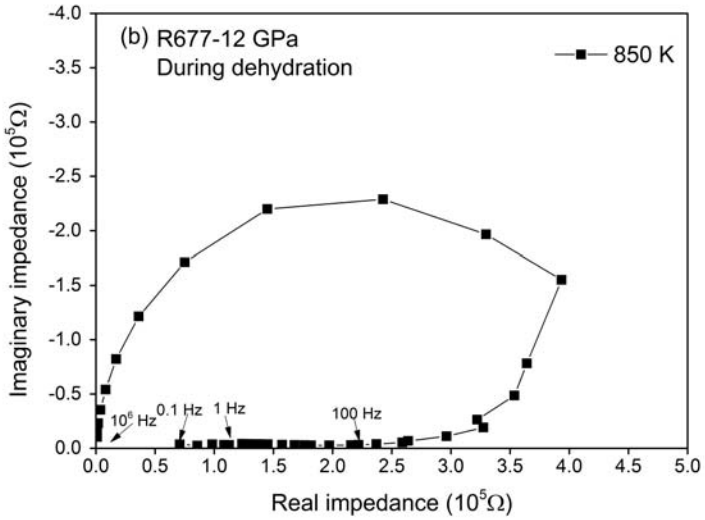

37

38 Figure DR3. Impedance spectrum of phengite (a) prior to and (b) during its dehydration.

39

40

41

42

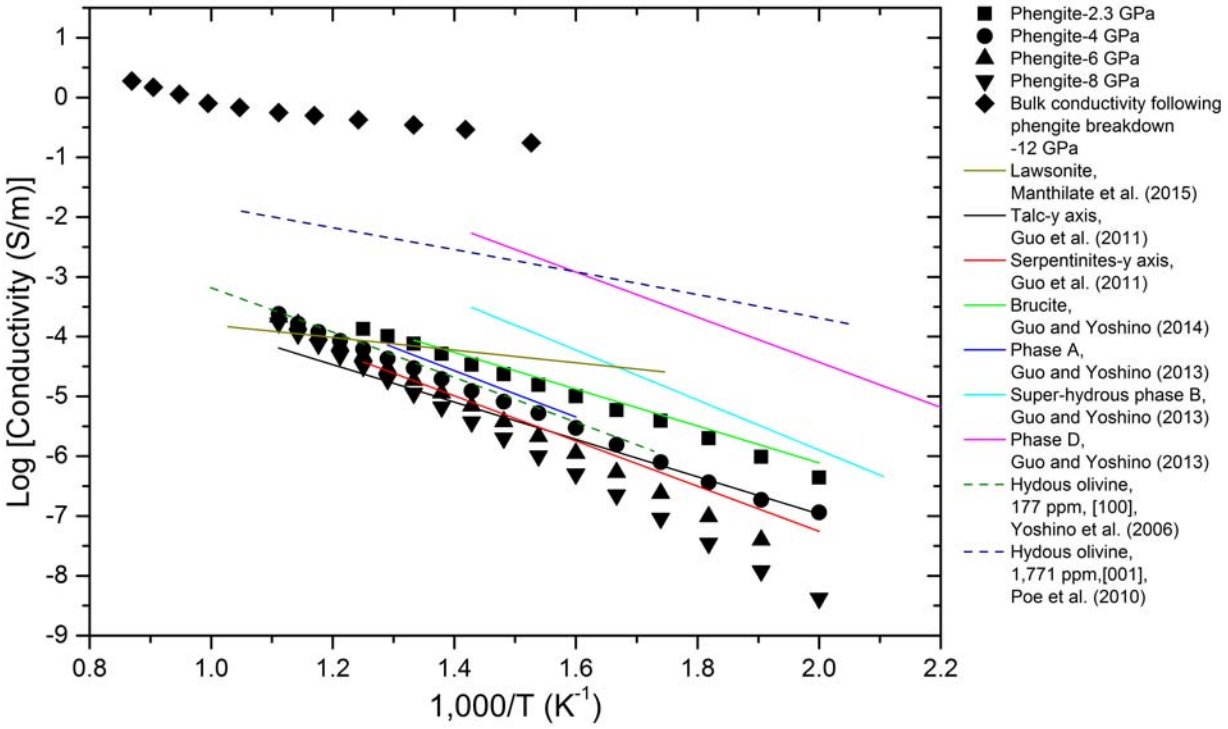

Figure DR4. Comparison between electrical conductivity of phengite and other minerals. Solid lines in dark yellow, back, red, blue, green, light blue and purple represent the electrical conductivities of lawsonite (Manthilake et al. 2015), talc, serpentinites (Guo et al., 2011), brucite (Guo et al., 2014), phase A, super-hydrous phase B and phase D (Guo and Yoshino, 2013), respectively. Dash lines in yellow and blue represent electrical conductivities of hydrous olivine single crystal ([100]) containing 177 ppm water (Yoshino et al., 2006) and olivine single crystal ([001]) containing 1,771 ppm water (Poe et al., 2010), respectively.

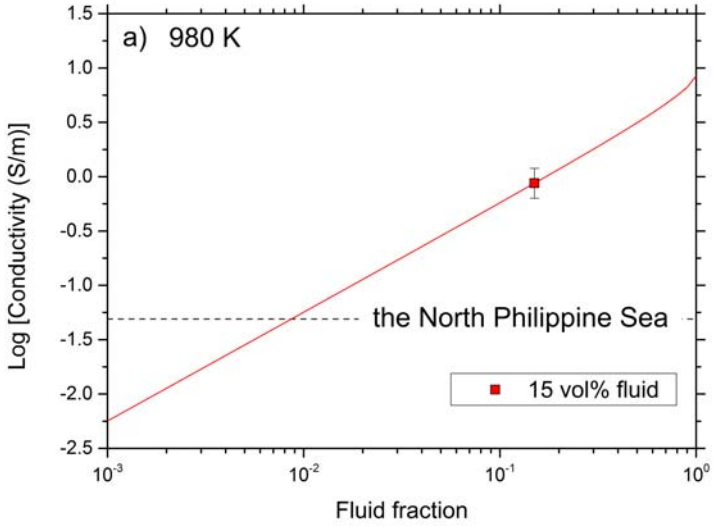

56

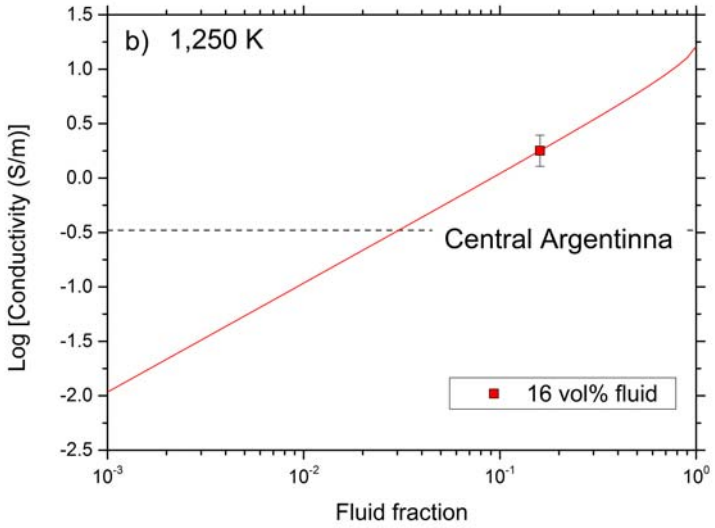

57

58

59 Figure DR5. Comparison between the conductivity values recorded by MT surveys and
60 experimental result following phengite breakdown at depth of a) 290 km (980 K in temperature)
61 in the North Philippine Sea and b) 280 km (1,250 K in temperature) in Central Argentina. Based
62 on the chemical equilibrium and mass balance, the upper limits of fluid fractions after phengite
63 breakdown are 15 vol% at 980 K and 10 GPa and 16 vol% at 1,250 K and 10 GPa, respectively,

with assumption that the fluid is only H_2O and the pressure effect on the conductivity is negligible. The density of solid phases is referred to Hacker et al. (2003) and Nishiyama et al. (2005), while the density of H_2O is referred to Franck (1970). Dehydration conditions are expected from the experiments results of basalt system (Schmidt, 1996) and the geotherms (Syracuse et al., 2010). The fluid fraction-log [conductivity] relationship was calculated by cube model (Waff, 1974). Conductivities observed by MT surveys: the North Philippine Sea (Tada et al., 2014) and Central Argentina (Burd et al., 2013)

87

TABLE DR1. CHEMICAL COMPOSITIONS OF THE STARTING MATERIAL AND THE RUN PRODUCTS

	Phengite (*n*=5)	K-hollandite (*n*=10)	Kyanite (*n*=5)	Garnet* (*n*=3)
SiO_2	51.83	66.84	37.09	41.40
TiO_2	0.28	0.15		0.02
Al_2O_3	24.11	21.14	62.29	23.44
FeO†	0.82	0.08	0.22	13.04
MnO		0.01		0.29
MgO	5.03	0.20	0.04	12.20
CaO		0.09	0.03	10.64
Na_2O	0.17	0.05	0.01	0.02
K_2O	10.59	11.97	0.05	0.05
Cr_2O_3		0.06	0.04	0.06
Total	92.83	100.57	99.77	101.15
Total O	10.00	8.00	5.00	12.00
Si	3.20	2.98	1.00	3.01
Ti				
Al	1.76	1.11	1.99	2.01
Fe	0.04		0.01	0.79
Mn				0.02
Mg	0.46	0.01		1.32
Ca				0.83
Na				
K	0.84	0.68		
Cr				
Total	6.33	4.80	3.00	7.99

Note: n is the total number of analyzed points.
*Garnet compositions are measured from the core
†It is assumed that iron is ferrous iron.

88
89
90
91
92
93

References

Burd, A. I., Booker, J. R., Mackie, R., Pomposiello, C., and Favetto, A., 2013, Electrical conductivity of the Pampean shallow subduction region of Argentina near 33 S: Evidence for a slab window: Geochemistry Geophysics Geosystems, v. 14, no. 8, p. 3192–3209.

Franck, E., 1970, Water and aqueous solutions at high pressures and temperatures: Pure and applied Chemistry, v. 24, no. 1, p. 13-30.

Guo, X., Yoshino, T., and Katayama, I., 2011, Electrical conductivity anisotropy of deformed talc rocks and serpentinites at 3 GPa: Physics of the Earth and Planetary Interiors, v. 188, no. 1-2, p. 69–81.

Guo, X., and Yoshino, T., 2013, Electrical conductivity of dense hydrous magnesium silicates with implication for conductivity in the stagnant slab: Earth and Planetary Science Letters, v. 369, p. 239–247.

Guo, X., and Yoshino, T., 2014, Pressure-induced enhancement of proton conduction in brucite: Geophysical Research Letters, v. 41, no. 3, p. 813–819.

Hacker, B. R., Abers, G. A., and Peacock, S. M., 2003, Subduction factory 1. Theoretical mineralogy, densities, seismic wave speeds, and H_2O contents: Journal of Geophysical Research-Solid Earth, v. 108, no. B1.

Manthilake, G., Mookherjee, M., Bolfan-Casanova, N., and Andrault, D., 2015, Electrical conductivity of lawsonite and dehydrating fluids at high pressures and temperatures: Geophysical Research Letters, v. 42, no. 18, p. 7398–7405.

Nishiyama, N., Rapp, R. P., Irifune, T., Sanehira, T., Yamazaki, D., and Funakoshi, K., 2005, Stability and P-V-T equation of state of $KAlSi_3O_8$-hollandite determined by in situ X-ray

observations and implications for dynamics of subducted continental crust material: Physics and Chemistry of Minerals, v. 32, no. 8-9, p. 627–637.

Poe, B. T., Romano, C., Nestola, F., and Smyth, J. R., 2010, Electrical conductivity anisotropy of dry and hydrous olivine at 8 GPa: Physics of the Earth and Planetary Interiors, v. 181, no. 3-4, p. 103–111.

Schmidt, M. W., 1996, Experimental constraints on recycling of potassium from subducted oceanic crust: Science, v. 272, no. 5270, p. 1927–1930.

Syracuse, E. M., van Keken, P. E., and Abers, G. A., 2010, The global range of subduction zone thermal models: Physics of the Earth and Planetary Interiors, v. 183, no. 1-2, p. 73–90.

Tada, N., Baba, K., and Utada, H., 2014, Three-dimensional inversion of seafloor magnetotelluric data collected in the Philippine Sea and the western margin of the northwest Pacific Ocean: Geochemistry Geophysics Geosystems, v. 15, no. 7, p. 2895–2917.

Waff, H. S., 1974, Theoretical considerations of electrical conductivity in a partially molten mantle and implications for geothermometry: Journal of Geophysical Research, v. 79, no. 26, p. 4003-4010.

Yoshino, T., Matsuzaki, T., Yamashita, S., and Katsura, T., 2006, Hydrous olivine unable to account for conductivity anomaly at the top of the asthenosphere: Nature, v. 443, no. 7114, p. 973–976.